ARTICLES

Bacterially Produced Manganese Oxide and Todorokite: UV Raman Spectroscopic Comparison

Hack-Sung Kim and Peter C. Stair*

Institute for Environmental Catalysis, Center for Catalysis & Surface Science, and Department of Chemistry, Northwestern University, Evanston, Illinois 60208

Received: March 17, 2004; In Final Form: August 31, 2004

UV Raman spectroscopic data measured at two distinct conditions, low and high laser power, establish that the manganese oxide (SP6-MnO_x) produced by the freshwater bacterium (*Leptothrix discophora* SP-6) closely resembles the 3 × 3-tunnel todorokite among the MnO_2 materials studied. Under the two conditions, the effect of hydration/cation and the phase transition of todorokite or SP6-MnO_x to Mn_3O_4 or birnessite will be described. A higher concentration of Mg^{2+} incorporated in the framework of the SP6-MnO_x than in todorokite is probably responsible for the formation of a new Raman band obtained at high laser powers, matching the most intense UV Raman band of synthetic birnessite. Also, we present the assignment of Raman bands for todorokite mineral and discuss the mutual exclusion principle that should hold for all the MnO_2 materials studied. These experiments provide characterization of hydrous, poorly crystalline, or nanocrystalline metal oxides, which are frequently difficult to identify.

Introduction

The synthesis and investigation of new (porous) manganese oxides is the focus of intensive research because of their promising properties as adsorbents, catalysts, chemical sensors, and battery materials.[1−3] Most of the common methods for synthesis of high surface area nanoscale materials are energy-inefficient, require harsh conditions (e.g., high temperature and pressure), and often produce toxic byproducts.[4] However, biological catalytic reactions are efficient, highly selective, performed under mild conditions (e.g., aqueous environments), and much faster than abiotic catalysis (e.g., by up to 10^5 times for the Mn(II) oxidation).[5] Klaus et al. reported potential uses of bacteria (*P. stutzeri* AG259) for Ag-based nanostructured thin film synthesis.[6] Using TEM, EXAFS, and UV Raman spectroscopy, we recently showed[7] that a Mn(II)-oxidizing freshwater bacterium produces the nanoscale, 3 × 3-tunnel todorokite-like MnO_2, which may have potential applications for the biosynthesis of nanocrystalline, porous manganese oxides.

The most common method for identifying the structure of MnO_x materials has been X-ray diffraction (XRD). In the field of mineralogy, MnO_x minerals formed in aqueous systems are typically hydrated, nanocrystalline, and poorly crystalline.[8] Furthermore, several minerals give almost the same XRD patterns.[9] Thus, the structural refinement using XRD is often crude or incomplete. X-ray absorption spectroscopy (XAS = XANES, X-ray absorption near-edge structure + EXAFS) has been extensively used to study the average local structure of manganese in various MnO_x minerals.[9−11] However, the application of XAS for characterizing the structure of bacterially produced MnO_x is limited because of the difficulty in distinguishing several MnO_x materials with similar spectral features. Vibrational (IR and Raman) spectroscopy is complementary to EXAFS in studying the MnO_x local structure[7] and is sensitive to the crystal symmetry and the local environments such as hydrogen bonding, which is especially important for the hydrated crystals. Raman spectroscopy has an important advantage over IR absorption spectroscopy for the study of aqueous (biological and hydrated geochemical) samples; water is a poor Raman scatterer, but liquid water absorbs IR radiation so strongly that IR absorption from the water frequently screens the vibrational information from the sample of interest. However, vibrational Raman spectroscopy has not been widely applied to study MnO_2 minerals[12] or bacterially produced manganese oxides compared to XAS.[13] This is probably because the dark colored (brown or black) MnO_2 materials strongly absorb visible light, so the Raman spectra of the samples are generally difficult to obtain. Nevertheless, Raman spectroscopy has been successfully used to probe the local structure of MnO_2 battery materials[14−17] and MnO_2 minerals.[15,18] Because UV Raman spectroscopy has advantages over conventional visible Raman spectroscopy, it has been used to study metal oxides[19] and biological samples.[20,21] We recently showed that UV Raman spectroscopy is more sensitive than EXAFS in distinguishing among the structures of several manganese oxides studied.[7] Here, we present a detailed analysis of the UV Raman data, showing that the UV Raman spectra from SP6-MnO_x and 3 × 3-tunnel todorokite are very similar.

Experimental Section

SP-6 Bacteria and SP6-MnO_x. Liquid culture of *Leptothrix discophora* SP-6 (ATCC 51168) was grown at room temperature

* To whom correspondence should be addressed. E-mail: pstair@northwestern.edu.

10.1021/jp048810a CCC: $27.50
Published on Web 10/12/2004

TABLE 1: Vibrational Spectroscopic Features, Crystallographic Systems, and Crystallographic Point Groups of the Reference MnO_2 Materials[a]

minerals	wavenumber/cm^{-1}							
pyrolusite		384 (m)	482 (m)	**538 (s)**	610 (m)	666 (w)		this work
(tetragonal, $P4_2/mnm$, D_{4h}^{14})		376 (vw)	486 (w)	**538 (s)**		665 (s)	750 (vw)	vis Raman[18]
	340 (m)	390 (m)		**540 (s)**	620 (s)		730 (w)	IR[23]
ramsdellite				**526 (s)**	~580 (vw)	654 (m)	750 (m)	this work
(orthorhombic, $Pbnm$, D_{2h}^{16})				518 (m)	**580 (s)**	630 (s), 680 (w)	740 (w)	vis Raman[18]
		392 (wm)	490 (w)	523 (m)	**576 (ms)**	650 (ms)	775 (vw)	vis Raman[15]
	270 (w)	375 (w)	475 (s)	**523 (s)**	595 (m)	690 (m)	750 (m)	IR[23]
cryptomelane		321 (m)	**467 (s)**	571 (w)				this work
(tetragonal, $I4/m$, C_{4h}^5)		310 (w)	475 (m)	**525 (s)**	590 (m)	705 (m)		IR[23]
chalcophanite	330 (w)	392 (m)	450 (w)	500 (w), 560 (vw)	**673 (m)**			this work
(rhombohedral, $R\bar{3}$, C_{3i}^2)	320 (w)	340 (w)	**440 (s)**, 475 (m), 495 (s)	530 (m), 590 (w)	620 (w), 670 (w)	810 (vw)		IR[23]
todorokite	310 (vw)[b]				**620 (s)**			this work
(monoclinic, $P2/m$, C_{2h}^1)			**430 (s)**	510 (s), 550 (s)	640 (w)	770 (w)		IR[23]
Na−OL-1	321 (w)	399 (vw)	467 (w)	**564 (s)**				this work
(triclinic, $P\bar{1}$, C_i)			467 (w)	510 (vw)		**706 (s)**		IR[31]

[a] Because the IR band positions are not given explicitly within the reported paper,[23,31] the IR frequencies summarized are rough estimates. Bold digits indicate the strongest band position in each vibrational spectrum of the materials (key: vw, very weak; w, weak; m, medium; s, strong; wm, weak to medium; ms, medium to strong). The "wm" and "ms" show the variable intensities depending on the conditions (the laser power used, the degree of hydration, and the orientation of the crystalline minerals). [b] Taken from the Raman spectrum of the todorokite mixture.

in MSVP/no-Fe medium (mineral salts, vitamins, and pyruvate; ATCC Culture Medium 1917 with no iron added), which consists of $(NH_4)_2SO_4$ (1.82 mM), $MgSO_4 \cdot 7H_2O$ (0.24 mM), $CaCl_2 \cdot 2H_2O$ (0.41 mM), KH_2PO_4 (0.15 mM), Na_2HPO_4 (0.21 mM), HEPES (10.00 mM, buffer, *N*-2-hydroxyethylpiperazine-*N*′-2-ethanesulfonic acid), Na-pyruvate (9.06 mM, $C_6H_6O_6Na$) as a carbon source, and a trace amount of several vitamins. The culture was slowly shaken (<100 rpm) on a rotating shake table. When the culture reached the stationary phase after ~7 days, 0.15 mM of aqueous Mn^{2+} (as a stock solution of $MnSO_4$) was added to the culture and bacterially oxidized for 14 days at room temperature. MSVP is a buffered medium and the pH of the medium varies between 7.2 and 7.3 during the bacterial growth and MnO_x production.

Reference MnO_2 Materials. The reference MnO_2 minerals available from mineral collection companies were characterized by XRD to verify their identity. The minerals used in UV Raman spectroscopic measurements (along with their location of origin) are pyrolusite (Kisenge Mine, Zaire), ramsdellite (Mistake Mine, Yavapai County, Arizona), cryptomelane (Woodmine, Tennessee), chalcophanite (Mina Ojuela Mapimi, Durango, Mexico), todotokite (Sterling Mine, Ogdensburg, Sussex County, New Jersey). We used synthetic birnessite[22] (referred to as OL-1 or Na-OL-1) as an analogue of birnessite because a well-defined birnessite mineral was not available. OL-1 showed characteristic XRD band features of birnessite.

The minerals used in IR absorption spectroscopic measurements obtained by Potter and Rossman,[23] for comparison to our Raman data (see Table 1 and the main text), are listed along with the location where the minerals were found: pyrolusite (Nissan in Germany & Sierra County, New Mexico), ramsdellite (Chihuahua, Mexico), cryptomelane (Patagonia Mine, Arizona), chalcophanite (Sterling Hill, New Jersey), todotokite (Charco Redondo in Cuba & Bombay in India).

UV Raman Spectroscopy. The UV Raman spectrometer has been described elsewhere.[19,24] It consists of a Spex 1877 triple spectrograph with an imaging photomultiplier tube. The 244 nm laser excitation source for UV Raman scattering is a Lexel 95-SHG Ar^+ laser equipped with a frequency-doubling BBO (Beta Barium Borate, BaB_2O_4) crystal. An $AlMgF_2$ coated ellipsoidal reflector using the 180° scattering geometry collected the scattered light from the sample. The Raman frequency was calibrated using several reference liquids (chloroform, dichloromethane, acetonitrile) and a Hg lamp. All UV Raman spectra were recorded under ambient conditions.

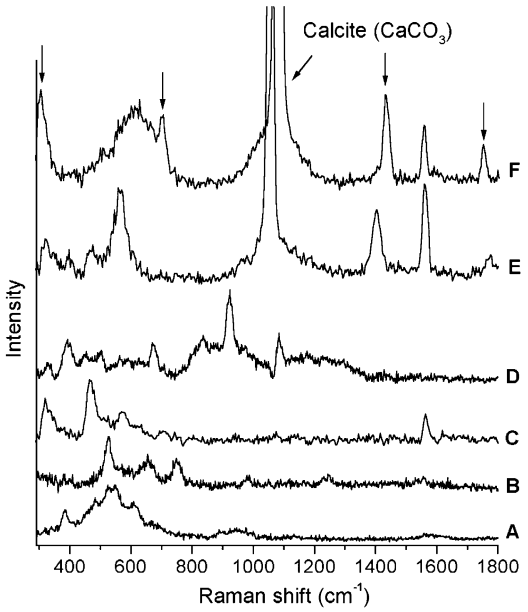

Figure 1. UV Raman spectra of several reference MnO_2 materials in the 290−1800 cm^{-1} region: (A) pyrolusite, (B) ramsdellite, (C) cryptomelane, (D) chalcophanite, (E) synthetic birnessite, and (F) todorokite. The UV Raman bands attributed to the calcite found in todorokite mineral are denoted with arrows in trace (F). The band centered at 1558 cm^{-1} is attributed to the O−O stretching vibration of neutral O_2 gas present in ambient condition.

Results and Discussion

1. Raman Spectra of the Reference MnO_2 Materials. Because XANES spectra[25] showed that the average oxidation state of Mn in SP6-MnO_x is ~3.8, we compare SP6-MnO_x to reference MnO_x materials with approximately +4 oxidation state of Mn using UV Raman spectroscopy (Figure 1). Because Mn atoms in manganese dioxides are always 6-fold coordinated,[10] the Raman bands of MnO_2 materials depend on the MnO_6 octahedral environments (e.g., edge/corner sharing, Jahn−Teller

distortion, interaction with water/cations in the tunnels or layers of MnO_2 materials). Their Raman frequencies in the 500−700 and 200−500 cm^{-1} range have been assigned[18] to the Mn−O stretching of MnO_6 octahedra and the Mn−O−Mn bending vibration in the MnO_2 octahedral lattice, respectively.

1.1. Pyrolusite and Ramsdellite. The UV Raman data from 1 × 1-tunnel pyrolusite (Figure 1A) and 1 × 2-tunnel ramsdellite (Figure 1B) are in good agreement in terms of positions with published visible Raman data,[15,18] as shown in Table 1. Bernard et al.[15] observed that the relative intensities of Raman bands of pyrolusite and ramsdellite in the region below 800 cm^{-1} were sensitive to the laser power used, the degree of hydration, and the orientation of the crystalline minerals. We summarize their visible Raman data from ramsdellite in Table 1. Hence, the differences in relative intensities between our UV Raman data and the reported visible Raman data are likely due to the differing excitation wavelength, laser powers used in the measurements, and possibly the degree of hydration in the minerals. Also, we summarize the reported IR absorption data[23] in the 200−1400 cm^{-1} region from pyrolusite and ramsdellite for comparison with our UV Raman data in Table 1. UV Raman positions and relative intensities of the bands centered at 538 cm^{-1} from pyrolusite and 526 cm^{-1} from ramsdellite match IR features of the band centered at ∼540 cm^{-1} and ∼523 cm^{-1} from corresponding minerals, respectively. Therefore, both the pyrolusite and ramsdellite measured here seem to violate the mutual exclusion principle, which we will discuss later.

1.2. Cryptomelane, Chalcophanite, and Synthetic Birnessite (Na-OL-1). The observed UV Raman (Figure 1C,D) and the reported IR absorption data[23] from 2 × 2-tunnel cryptomelane and layered chalcophanite are summarized in Table 1. The UV Raman bands of cryptomelane do not match the IR absorption data in regard to band position. This is because of the mutual exclusion principle, which we will discuss later.

A Raman band centered at 1080 cm^{-1} from chalcophanite (Figure 1D) is attributed to a calcite impurity; the band assignment of calcite will be described later. The two Raman bands centered at 835 and 923 cm^{-1} in Figure 1D are not attributed to chalcophanite. First, the layered chalcophanite ($ZnMn_3O_7 \cdot 3H_2O$) structure[26] consists of sheets of edge sharing MnO_6 octahedra alternating with layers of Zn cations and water molecules in the stacking sequence (···Mn−O−Zn−H_2O−Zn−O−Mn···). The Zn cations are coordinated to three lattice oxygen atoms and three water oxygen atoms. Because the Mn−O internal (stretching and bending) vibrations in the MnO_2 materials have been observed[18] below 800 cm^{-1}, the two Raman bands could only be attributed to the Zn−O related vibration. However, the Raman data from model compounds with the same octahedral coordination as chalcophanite such as $ZnWO_4$ and $Zn(H_2O)_6$ show that the two Raman bands do not correspond to the Zn−O related vibration. The $ZnWO_4$ (C_{2h} crystallographic point group, wolframite structure)[27] is an octahedrally coordinated Zn compound[28] and the Zn−O bond length[29] in the $ZnWO_4$ is exactly the same (2.1 Å) as the mean bond length of Zn−O in chalcophanite.[26] The Zn−O force constant is much smaller than W−O force constant and the Raman bands of Zn−O related vibration in the $ZnWO_4$ were observed[29] to be less than 490 cm^{-1}. Additionally, the highest Raman frequency (ν_1) of the $Zn(H_2O)_6$ belonging to the octahedral O_h group was shown[30] to be less than 400 cm^{-1}. Therefore, all the Raman bands of the Zn−O related vibration are expected to be less than ∼500 cm^{-1}. Second, the two bands are not likely to be attributed to the combination/overtone of lattice (external) vibration because the band centered at 923 cm^{-1} is intense. The two Raman bands are not currently identified and may be due to impurities included in the chalcophanite mineral.

The observed UV Raman (Figure 1E) and the previous IR absorption data[31] of layered Na-OL-1 are summarized in Table 1. The chemical formula,[22] crystallographic system,[32] and the average oxidation state of Mn in the synthetic birnessite (Na-OL-1) are $K_{0.005}Na_{0.39}Mg_{0.042} \cdot 0.044MgO \cdot MnO_{1.76} \cdot 0.77H_2O$, triclinic with space group $P\bar{1}$, and 3.52, respectively. The two strong bands centered at 1055 and 1402 cm^{-1} in the Raman spectrum of Na-OL-1 are attributed to a nitrate impurity and are in good agreement with the symmetric and asymmetric stretching vibration of nitrate in solid $NaNO_3$, respectively.[33,34] Because nitrate is a strong Raman scatterer (large polarizability change during vibration), traces of nitrate give distinct Raman bands. The nitrate originates from $NaNO_3$ that was used as the Na^+ source in the synthesis.[35]

1.3. Todorokite: Estimated Raman Band Position. The UV Raman bands from 3 × 3-tunnel todorokite are shown in Figure 1F. The bands denoted with arrows centered at 305 cm^{-1} (E_g), 705 cm^{-1} (E_g, ν_4), 1080 cm^{-1} (A_{1g}, ν_1), 1433 cm^{-1} (E_g, ν_3), and 1752 cm^{-1} ($2\nu_2$) are attributed to the calcite impurity found in todorokite mineral. Because carbonate as well as nitrate is a very strong Raman scatterer, traces of carbonate in todorokite mineral give distinct Raman bands. Calcite (D_{3d}^6 space group) and aragonite (D_{2h}^{16} space group) crystals have the same composition, $CaCO_3$. However, the site symmetry of the carbonate ion in calcite and aragonite is D_3 and C_s, respectively.[36] The absence of the UV Raman band centered at 852 cm^{-1} (ν_2) confirms that the carbonate is calcite (common $CaCO_3$), not aragonite.[36] UV Raman spectral features of the calcite are in good agreement with the visible Raman data reported previously.[37−39]

A strong band centered at 620 cm^{-1} in the Raman spectrum of todorokite (Figure 1F) matches well with the expected Raman frequencies of todorokite. Potter and Rossman reported that a decrease in the IR frequency of major bands in the 300−700 cm^{-1} range measured from manganese oxide minerals correlated with an increase in the number of shared edges per MnO_6 octahedron.[23] They suggested that todorokite should have ∼5 shared edges per MnO_6 on the basis of the correlation although the structure of todorokite was not known at the time of their report. Their estimation was confirmed, and the average number of shared edges per MnO_6 octahedron in todorokite is known[40] to be 4.7. Similarly, Julien and Massot recently reported that a decrease in the Raman frequency associated with two sets of stretching modes (denoted ν_1 and ν_2) in the 500−700 cm^{-1} range measured from manganese oxide minerals correlated with an increase in the number of shared edges per MnO_6 octahedron.[18] The frequency of the strongest (ν_1) Raman band is inversely proportional to the number of shared edges per MnO_6 octahedron. Although todorokite was not included in their correlation, it indicates that both of the ν_1 and ν_2 Raman frequencies for manganese oxide with 4.7 shared edges per MnO_6 octahedron should be in the range ∼600−610 cm^{-1}. Therefore, our measured UV Raman spectrum from todorokite is in good agreement with the expected Raman frequencies for todorokite.

1.4. Mutual Exclusion Principle. The space groups of monoclinic todorokite,[1] trigonal (=rhombohedral) chalcophanite,[26] triclinic OL-1,[32] body-centered tetragonal cryptomelane,[1,41,42] orthorhombic ramsdellite,[1,43,44] and tetragonal pyrolusite[1,44] are known to be $P2/m$ ($=C_{2h}^1$ crystallographic point group), $R\bar{3}$ ($=C_{3i}^2$), $P\bar{1}$ ($=C_i$), $I4/m$ ($=C_{4h}^5$), $Pbnm$ ($=D_{2h}^{16}$), and $P4_2/mnm$ ($=D_{4h}^{14}$), respectively. Because the six crystallographic point groups have an inversion center as a symmetry operation, the

irreducible representations transform to *g* and *u* types, i.e., even or odd under the inversion operation. According to the mutual exclusion principle, in crystals with an inversion center, Raman active modes transform as *g* representations and IR modes as *u* representations; i.e., Raman- and IR-active modes have different frequencies except for accidental degeneracies. Our observations, as shown in Table 1, demonstrate that the mutual exclusion principle holds rigorously (IR and Raman frequencies do not have any similarity with each other) for todorokite and cryptomelane and holds approximately (inactive modes appear weakly or very weakly) for the layered chalcophanite and OL-1. A weak UV Raman and IR band centered at ~467 cm^{-1} of Na-OL-1 and a UV Raman band centered at 673 cm^{-1} with an IR band centered at ~670 cm^{-1} of chalcophanite (Table 1) are probably the same vibrational mode although the same frequency might result from accidental degeneracy. The reason for the violation of the rigorous exclusion principle is likely to be a small deviation of the inversion center possibly owing to structural defects (e.g., cation disorder). For example, violation of the exclusion principle has been observed in the liquid-phase owing to the collision-induced instantaneous breaking of inversion symmetry.[45]

The mutual exclusion principle seems not to hold within pyrolusite and ramsdellite on the basis of our observation. The observed UV Raman bands centered at 538 cm^{-1} and the published IR bands centered at ~540 cm^{-1} of pyrolusite seem to be due to the same normal mode of vibration (see Table 1). Because the IR band positions are not given explicitly within the paper,[23] the IR frequencies summarized in Table 1 are estimated from the published figures of IR spectra. XRD analysis[23] identified that pyrolusite has two structural forms, i.e., tetragonal and orthorhombic modification (β-modification).[3] The space group[3] of the orthorhombic modification is *Pnma* and its crystallographic point group[36] is D_{2h}. Because D_{2h} also has an inversion center as a symmetry operation, the mutual exclusion principle should hold for the orthorhombic pyrolusite as well as tetragonal pyrolusite. Therefore, pyrolusite mineral, which has two structural forms, probably includes structural defects to break the inversion symmetry.

Because the crystallographic point group of ramsdellite is known to be D_{2h}, the unit cell of ramsdellite has an inversion center of symmetry and the mutual exclusion principle should hold within the ramsdellite. However, the observed UV Raman bands centered at 526 and 750 cm^{-1} and the published IR band centered at ~523 and ~750 cm^{-1} of ramsdellite, respectively, (Table 1) seem to be due to the same normal mode of vibration. Julien and Massot[18] reported a visible Raman band centered at 518 cm^{-1} and an IR absorption band centered at 517 cm^{-1} from ramsdellite. Their visible Raman data are in good agreement with our UV Raman data and also show the breakdown of the exclusion principle although they did not discuss this. The violation of the mutual exclusion principle has been observed in single crystals, and it was suggested to be caused by cation disorder that leads to a breakdown of the inversion center.[46,47] Although it is not clear why the mutual exclusion principle did not hold within the ramsdellite, the possible reason could be either an accidental degeneracy or the lack of the inversion center possibly owing to the presence of structural defects (e.g., cation disorder). The latter reason seems to be more likely because two frequencies in the Raman and IR spectra of ramsdellite are the same. Ramsdellite is thermodynamically unstable,[3] which might be the reason for the possible structural defects.

1.5. Raman Bands Assignment of Todorokite. The vibrational analysis of crystals can be performed by site group analysis, factor group analysis, and the correlation method, with the three methods giving the same result.[36] To our knowledge, the vibrational band assignments for todorokite mineral have not been performed as yet. Here we briefly describe the Raman band assignments of todorokite using the reported factor group analysis of the chain-structured solid CF_3COOH. The space group of todorokite and the solid CF_3COOH is the same, *P*2/*m*. The factor group of *P*2/*m* is C_{2h} and the representation of the internal vibrations of the CF_3COOH is[48] $\Gamma_{int}(C_{2h}) = 12A_g + 6B_g + 6A_u + 12B_u$. The mutual exclusion principle holds within the CF_3COOH and in-phase vibrations (A_g and B_g) are Raman active, whereas out-of phase modes (A_u and B_u) are IR active. Although the number of internal vibrational modes of todorokite is different from solid CF_3COOH, the Raman active modes for todorokite should also consist of the same symmetry species (A_g and B_g) as the solid CF_3COOH because the factor groups of todorokite and solid CF_3COOH are the same.

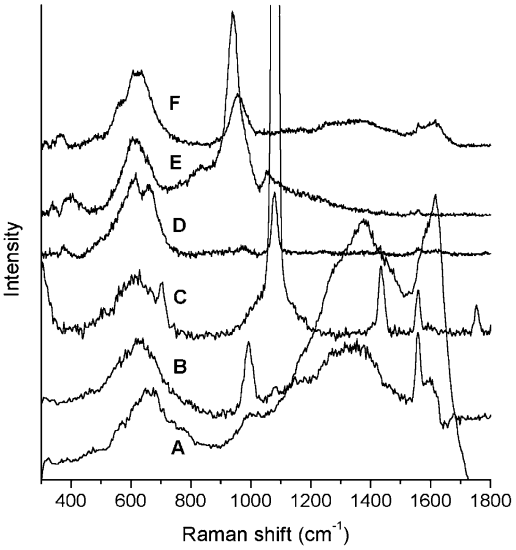

Figure 2. UV Raman spectra of todorokite mineral (C, D), the todorokite mixture (B, E), and SP6-MnO_x (A, F) in the 300−1800 cm^{-1} region when the laser power was low (LP, ~2 mW, A−C) and high (HP, ~22 mW, D−F). The UV Raman spectrum of todorokite mineral as shown in Figure 1F is reproduced in trace (C). The Raman bands in traces (C) and (D) centered at 305, 705, 1080, 1433, and 1752 cm^{-1} (denoted with arrows in Figure 1F) are attributed to the calcite impurity found in todorokite mineral. The band centered at 1558 cm^{-1} is attributed to the O−O stretching vibration of neutral O_2 gas present in ambient condition.

We assign the strong Raman band of todorokite centered at 620 cm^{-1} (Figure 1F and Figure 2C) to the A_g mode (Mn−O symmetric stretching of the MnO_6 octahedral) and a very weak band centered at 310 cm^{-1} in the Raman spectrum of the todorokite mixture (Figure 2B, not shown in Figure 1F and Figure 2C owing to the overlapping by a strong band centered at 305 cm^{-1} attributed to calcite), to the B_g mode (Mn−O−Mn bending vibration in the MnO_2 octahedral lattice) for the following reasons. First, the Mn−O (internal) stretching vibration of MnO_6 octahedra and the Mn−O−Mn bending vibration in the MnO_2 octahedral lattice was observed (and calculated)[16,18] in the ~550−700 and ~200−500 cm^{-1} range, respectively. Second, the lattice (external) vibrational frequencies[36] are usually lower than 300 cm^{-1}. Although they may appear at higher frequency as combination/overtone bands, they should appear *with* internal modes.[36] Because a band centered at 620 cm^{-1} is the only band in the high-frequency region (~550−700 cm^{-1}) and quite intense, the band is not likely to be the combination/

overtone of the external vibration. Third, Raman active modes for todorokite consist of A_g and B_g internal vibrations on the basis of the above factor group analysis. Fourth, the totally symmetric stretching (A_g) vibration of MnO_6 octahedra normally appears as the strongest Raman band.[36]

Interestingly, UV Raman spectral features of todorokite, 620 cm^{-1} (strong) and 310 cm^{-1} (weak), are very similar to published[16,17] Raman data of cubic spinel (space group $Fd3m$)[1] $LiMn_2O_4$, 625/631 cm^{-1} (strong) and 365/343 cm^{-1} (weak). Ammundsen et al.[16] assigned the strongest Raman band centered at 625 cm^{-1} of the $LiMn_2O_4$ (O_h^7 crystallographic point group)[1] to the symmetric A_{1g} on the basis of their theoretical calculation. Tetragonal spinel $Li_2Mn_2O_4$ (605, 398 cm^{-1}) and monoclinic layered $LiMnO_2$ (603, 481/422 cm^{-1}) also show similar Raman spectral features. Several similarities between todorokite and cubic spinel $LiMn_2O_4$ include the average oxidation number of Mn, atomic ratio of Mn to oxygen, and crystal structure (three-dimensional 1×3-tunnel[1] and one-dimensional 3×3-tunnel). Because the cubic spinel $LiMn_2O_4$ structure can be regarded[18] as being composed of MnO_6 octahedra and LiO_4 tetrahedra, it consists of the same MnO_6 octahedra as todorokite. On the basis of the Raman correlation,[18] as we discussed above, we estimate that the number of shared edges per MnO_6 octahedron in cubic spinel $LiMn_2O_4$ is 4.0−4.5, close to 4.7, the number in todorokite.

2. Raman Spectra of SP6-MnO_x Obtained at Low and High Laser Power. Figure 2 compares the UV Raman spectrum of SP6-MnO_x (mixed with the MSVP consumed by bacteria) with those of todorokite mineral and the todorokite mixture (mixed with the MSVP consumed by bacteria) when the laser power was low (LP, 2 mW) and high (HP, 22 mW). Because the todorokite mixture and SP6-MnO_x include the growth medium (MSVP), we obtained the UV Raman spectra of the individual components of the MSVP, not shown in this report, and compared them to the Raman spectra of the two samples. The water content was minimized in the two samples in order to maximize the Raman signal. The Raman bands centered at ∼1350/1600 cm^{-1} (Figure 2A,B,F) and 940−990 cm^{-1} (Figure 2A,B,E,F) are due to the organic compounds (HEPES and pyruvate) and HPO_4^{2-} found in the MSVP, respectively.

Major differences between the two sets of Raman spectra measured at LP and HP conditions below ∼1000 cm^{-1} are the red shift of the bands appearing at 990 cm^{-1} (to 940−955 cm^{-1}) and at 620−660 cm^{-1} (to 615−623 cm^{-1}), the reduced width of the band centered at 620−660 cm^{-1}, and the appearance of the two new bands centered at 657 and 560 cm^{-1}.

2.1. Phase Transition to Mn_3O_4 at HP Condition and Gaussian Curve Fitting. The UV Raman bands of todorokite mineral measured at LP and HP conditions are shown in Figure 2C,D, respectively. The difference in the relative intensities of the bands from calcite (1080 cm^{-1}, etc.) with respect to the band centered at 615−620 cm^{-1} is attributed to the different location of todorokite mineral between the two conditions. A major difference between the two sets of Raman spectra measured at LP and HP conditions is the appearance of a new band centered at 657 cm^{-1}. Only the todorokite mineral shows a distinct Raman band (shoulder) centered at 657 cm^{-1} and a weak band centered at 373 cm^{-1} under the HP condition (Figure 2D), which are characteristic Raman features of Mn_3O_4. Many MnO_2 materials (e.g., coronadite, romanechite, todorokite, etc.) transform to Mn_3O_4 when irradiated with high laser power[49] or heated[50] above 600 °C. Mn_3O_4 is thermodynamically stable in air[51] even after prolonged heating at 1300 °C and thus has been synthesized[49] by heating MnO_2 at 1000 °C in air.

TABLE 2: Full Width at Half-Maxima (FWHM, in cm^{-1}) and the Relative Intensities of the Decomposed Bands Obtained by Gaussian Curve Fitting from the UV Raman Spectra Measured at HP Condition of Todorokite (Figure 2D), the Todorokite Mixture (Figure 2E), and SP6-MnO_x (Figure 2F) in the 500−800 cm^{-1} Range[a]

	decomposed bands and their origin		
	560 cm^{-1} OL-1	615 cm^{-1} dehydrated todorokite	657 cm^{-1} Mn_3O_4
todorokite	N/A	72 cm^{-1} (100)	36 cm^{-1} (31)
todorokite mixture	N/A	78 cm^{-1}	N/A
	N/A	73 cm^{-1} (100)	36 cm^{-1} (6.5)
SP6−MnO_x	28 cm^{-1} (10.5)	74 cm^{-1} (100)	N/A

[a] The relative intensities described in parentheses were obtained by integration of the decomposed bands and are normalized to that of the decomposed band centered at 615 cm^{-1}. The broad band centered at 615 cm^{-1} in the Raman spectrum of the todorokite mixture can be decomposed into one band or two bands. Band profiles are given in Figure 3.

Although the broad bands centered at 615−623 cm^{-1} of both SP6-MnO_x (Figure 2F) and the todorokite mixture (Figure 2E) measured at HP condition do not apparently include the characteristic Mn_3O_4 band centered at 657 cm^{-1}, they might have some contribution from a band centered at 657 cm^{-1} owing to their width. To investigate this, we used Gaussian curve fitting and the broad bands centered at 615−623 cm^{-1} measured at HP condition were decomposed into Gaussian profiles. Todorokite mineral is the most pure compound (except for a trace of calcite) of the three samples because the other two samples are mixtures including MSVP. Thus, it would be reasonable to assume that the full width at half-maxima (FWHM) of the band centered at ∼615 cm^{-1} (attributed to the todorokite in Figure 2E,F) for both the todorokite mixture and SP6-MnO_x should not be less than the FWHM of the decomposed band centered at 615 cm^{-1} (Figure 2D) for todorokite mineral. It would also be reasonable that the number of bands decomposed from trace 2D is 2 because a higher number of decomposed bands is arbitrary.[52] The acceptable number (based on the above assumption), position, FWHM, and intensities of the bands decomposed from traces Figure 2D−F in the 500−800 cm^{-1} range are given in Table 2, and the decomposed curve profiles are shown in Figure 3. The band profiles decomposed by Gaussian curve fitting from the Raman spectrum of todorokite mineral clearly show an intense band appearing at 657 cm^{-1}, as expected. The Raman band appearing at 615 cm^{-1} (Figure 2E) of the todorokite mixture can be decomposed into one or two bands (Table 2) by Gaussian curve fitting; i.e., some or no amount of the todorokite mixture was converted to Mn_3O_4, but no SP6-MnO_x was converted to Mn_3O_4 at the HP condition. This indicates that there is a strong interaction between the todorokite mineral (and SP6-MnO_x) and MSVP and that this interaction inhibited the phase transition of todorokite to Mn_3O_4. Hydrated cations (K^+, Na^+, Mg^{2+}, Ca^{2+}) found in the MSVP are probably responsible for the interaction, because cations are well-known to critically affect the phase transitions of todorokite-type manganese oxides.[53] The SP6-MnO_x mixture is visibly more homogeneous than the todorokite mixture and smaller (nanosized) SP6-MnO_x particles[7] may be responsible for the stronger interaction with MSVP (inhibition of the phase transition to Mn_3O_4).

2.2. Dehydration at HP Condition: Red Shift and Band Narrowing. Other major differences between the two sets of Raman spectra measured at LP and HP conditions below ∼1000 cm^{-1} are the red shift of the bands appearing at 990 cm^{-1} (to 940−955 cm^{-1}) and at 620−660 cm^{-1} (to 615−623 cm^{-1}) and

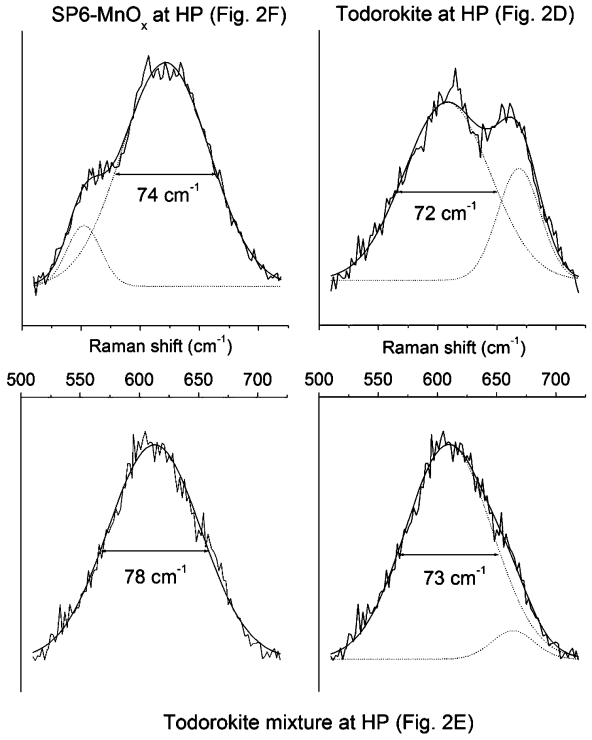

Figure 3. Band profiles decomposed by Gaussian curve fitting from the UV Raman spectra measured at HP condition of todorokite (Figure 2D), the todorokite mixture (Figure 2E), and SP6-MnO_x (Figure 2F) in the 500−800 cm^{-1} range. The full widths at half-maxima (FWHM) of the decomposed bands centered at ∼615 cm^{-1} (most intense) are indicated in the Figure and the relative intensities of decomposed bands are summarized in Table 2.

the reduced width of the band centered at 620−660 cm^{-1}. A Raman band appearing at 990 cm^{-1} (Figure 2A) of SP6-MnO_x under the LP condition was significantly red shifted (−35 cm^{-1}) to 955 cm^{-1} (Figure 2F) under the HP condition. A larger red shift (−50 cm^{-1} from 990 cm^{-1}) in the UV Raman spectrum of the todorokite mixture measured at the HP (Figure 2E) with respect to the LP condition (Figure 2B) was observed. Although Raman bands appearing at ∼990 cm^{-1} (Figure 2A,B) are attributed[54,55] to either the ν_1 stretching vibration of SO_4^{2-} or the PO_3 symmetric stretching of HPO_4^{2-}, Raman bands appearing at 940−955 cm^{-1} (Figure 2E,F) are attributed to the ν_1 stretching vibration of PO_3 symmetric stretching of HPO_4^{2-}. We observed that the most intense Raman bands from aqueous sulfates (e.g., $MnSO_4$, $MgSO_4$, and ammonium sulfate) at ∼975 cm^{-1} did not noticeably red shift compared to the corresponding Raman bands of solid sulfates; however, the most intense Raman band of aqueous Na_2HPO_4, observed at 980 cm^{-1}, did distinctly red shift to 931 cm^{-1} in the solid state. An IR absorption spectroscopic study[56] of aqueous and solid Na_2HPO_4 also showed a red shift (988 to 948 cm^{-1}) similar to our UV Raman data. Pessall et al.[54] reported that the most intense Raman band of anhydrous Na_2HPO_4 noticeably red shifted compared to the corresponding Raman band of aqueous Na_2HPO_4, thus supporting our observation. Therefore, the band position appearing at 940−990 cm^{-1} reflects the degree of the hydration, and the red shift is supporting evidence for dehydration at the HP condition. Similarly, the difference in position of the bands appearing at 620 cm^{-1} (Figure 2C), 630 cm^{-1} (Figure 2B), 660 cm^{-1} (Figure 2A) at LP condition are the result of different degrees of hydration (i.e., *hydrated* cations and water in the tunnels) because the three bands merge into a single band upon dehydration (i.e., HP condition).

Todorokite is a 3 × 3-tunnel MnO_2 with variable amounts of H_2O, Na^+, Ca^{2+}, and K^+ in the tunnels.[57] Water in the tunnels of synthetic todorokite is removed[53] at ∼300 °C, and the removal of water does not change the framework structure.[58] Our HP condition will raise the temperature at the focused spot on the sample high enough to remove most of the water in the todorokite and the todorokite mixture, but not high enough for the extensive phase transition of the samples to Mn_3O_4 because the todorokite and todorokite mixture were only partially converted to Mn_3O_4 at the HP condition.

The large width (FWHM ∼ 160 cm^{-1}) of the bands centered at 620−660 cm^{-1} (except for the band centered at 705 cm^{-1} attributed to calcite) in the three Raman spectra (Figure 2A−C) measured at the LP condition indicates the influence of hydrogen bonding in the environments of the Mn−O bond in todorokite and SP6-MnO_x (coordinated by several hydrated cations/water in the tunnels). Hydrogen-bonded materials have[59] broad vibrational bands with FWHM on the order of hundreds of cm^{-1}. The FWHM of the bands appearing at 620−660 cm^{-1} in the Raman spectra of all three samples are reduced upon dehydration (at HP condition) by a factor of 2 (from 160 to 72−78 cm^{-1}). Because the FWHM of the broad bands, even after dehydration, is larger than the corresponding band centered at 631 cm^{-1} from a similar MnO_2 material, cubic spinel $LiMn_2O_4$, the broad band may be overlapped by at least two decomposable bands. Both ν_1 and ν_2 modes of todorokite appear in this same range, as we explained above; however, we did not attempt to decompose the broad band because the numerical decomposition of a structureless contour is not unique.[52]

The FWHM of the bands appearing at 620−660 cm^{-1} in the Raman spectra of all the three samples are identical irrespective of the LP or HP condition. Therefore, the UV Raman spectrum of SP6-MnO_x is in good agreement with the todorokite mixture in terms of the FWHM as well as the position of Mn−O stretching band. Consequently, SP6-MnO_x most closely resembles todorokite among the MnO_2 materials studied using UV Raman spectroscopy.

2.3. A New Band Appearing at 560 cm^{-1}. Another difference between the two sets of Raman spectra measured at LP and HP conditions below ∼1000 cm^{-1} is the appearance of a new band centered at 560 cm^{-1}. Only the SP6-MnO_x shows a Raman band (shoulder) centered at 560 cm^{-1} at the HP condition (Figures 2F and 3 and Table 2). This suggests that the SP6-MnO_x and todorokite studied may have different concentrations of defects or cations in the framework. Although the stoichiometry of todorokite is typically described[60] as $(Na, Ca, K)_{x\sim0.3-0.7}(Mg,Mn)_6O_{12}\cdot nH_2O$, chemical analyses of todorokite minerals show considerable variation in the cation content depending on the mineral's location of origin.[61] Na^+, Ca^{2+}, K^+, and water are in the tunnels, and Mg^{2+} (or Cu^{2+}, Ni^{2+}) is in the framework of todorokite on the basis of the Rietveld refinement method.[57] Among the possible cations that could incorporate in the framework (Mg^{2+}, Cu^{2+}, Ni^{2+}), only Mg^{2+} is available from our MSVP solution. Therefore, the content of the cations in the tunnels and the concentration of Mg^{2+} in the framework of the todorokite mixture and SP6-MnO_x are unlikely to be the same.

Our HP condition partially transforms todorokite mineral to Mn_3O_4. Similarly, the new band is probably attributed to another manganese oxide partially transformed from the todorokite-like SP6-MnO_x. It has been reported that the thermal stability of todorokite-like manganese oxides (Mg-OMS-1) is affected by the Mg^{2+} concentration, and that Mg-OMS-1 starts to decompose at lower temperatures as the concentration of Mg^{2+} in the

framework increases.[53] We expect a similar trend in the todorokite-like SP6-MnO_x. The SP6-MnO_x started to decompose at temperatures induced by the HP condition where the todorokite mixture did not; therefore, SP6-MnO_x appears to have a higher concentration of Mg^{2+} in the framework than the todorokite mineral. The initial and final (consumed by bacteria) MSVP medium included a higher concentration of the cations (Na^+, Ca^{2+}, K^+, Mg^{2+}) that were available during the formation of the SP6-MnO_x.[62]

The distinct Raman band centered at 560 cm^{-1} matches well with the strong Raman band of Na-OL-1 in terms of position and width. The FWHM of the bands measured from the Raman spectrum of Na-OL-1 and decomposed (by Gaussian curve fitting) from the Raman spectrum of SP6-MnO_x are 33 cm^{-1} (Figure 1E) and 28 cm^{-1} (Table 2), respectively. Laberty et al. reported[63] that Na-OL-1 has the lowest enthalpy of formation (when the Na concentration in the layered structure is high enough) among all the octahedral manganese oxides studied (e.g., ΔH_f(Mg-OMS-1) = −22.8 kJ/mol, ΔH_f(Na-OL-1) = −65.6 kJ/mol) using high-temperature solution calorimetry. The Na concentration in our experiment was high enough to stabilize Na-OL-1. Because the phase transition of the todorokite-type OMS-1 to the birnessite-type OL-1 is thermodynamically favored, the birnessite-type layered structure is likely formed from the todorokite structure at the HP condition. Birnessite and todorokite are the two most abundant manganese oxide minerals in terrestrial deposits and ocean nodules.[64] Takematsu et al.[65] observed that highly oxidizing seawater environments induced by oxygenated hydrothermal fluids transformed todorokite into birnessite. Our HP condition may mimic these highly oxidizing environments.

Conclusion

This paper follows up our previous communication[7] that describes the characterization of bacterial MnO_x (SP6-MnO_x) structure using combined transmission electron microscopy (TEM), extended X-ray absorption fine structure (EXAFS), and UV Raman spectroscopy. Because XANES data[25] showed that the oxidation number of Mn in SP6-MnO_x is almost 4, only the reference Mn oxides with approximately +4 oxidation state of MnO_x were compared with the SP6-MnO_x using EXAFS and UV Raman spectroscopy. Here we described a detailed analysis of UV Raman data measured at two distinct conditions, low and high laser power, and established that the manganese oxide (SP6-MnO_x) produced by the freshwater bacterium (*Leptothrix discophora* SP-6) closely resembles the 3 × 3-tunnel todorokite among the MnO_2 materials studied.

The assignment of Raman bands for todorokite mineral, the mutual exclusion principle that should hold for the MnO_2 materials, the phase transition of todorokite or SP6-MnO_x to Mn_3O_4 or birnessite, and the effect of hydration/cation and the concentration of Mg^{2+} incorporated in the framework of the SP6-MnO_x and in todorokite were presented and discussed.

Acknowledgment. We thank Prof. Pablo A. Pastén, Prof. Jean-François Gaillard, Dr. Peter Wightman, and Joo-Hyoung Lee for helpful discussions, Prof. Steven Suib for supplying the synthetic birnessite (Na-OL-1), and Dr. Jason Pless for a careful reading of this manuscript. This work was supported by the Director of the Chemistry Division, Basic Energy Science, U.S. Department of Energy, Grants DE-FG02-97ER14789 and DE-FG02-03ER15457, and by the EMSI program of the National Science Foundation and the Department of Energy (CHE-9810378) at the Northwestern University Institute for Environmental Catalysis.

References and Notes

(1) Feng, Q.; Kanoh, H.; Ooi, K. *J. Mater. Chem.* **1999**, *9*, 319.
(2) Suib, S. L. *Chem. Innovation* **2000**, *30*, 27.
(3) Albering, J. H. Structural Chemistry of Manganese Dioxide and Related Compounds. In *Handbook of Battery Materials*; Besenhard, J. O., Ed.; Wiley-VCH: Weinheim, Germany, 1999.
(4) Sarikaya, M. *Proc. Natl. Acad. Sci. U.S.A.* **1999**, *96*, 14183.
(5) Nealson, K. H.; Tebo, B. M.; Rosson, R. A. Occurrence and mechanisms of microbial oxidation of manganese. In *Advances in Applied Microbiology*; Laskin, A. I., Ed.; Academic Press: San Diego, 1988; Vol. 33, p 279.
(6) Klaus, T.; Joerger, R.; Olsson, E.; Granqvist, C.-G. *Proc. Natl. Acad. Sci. U.S.A.* **1999**, *96*, 13611.
(7) Kim, H.-S.; Pastén, P. A.; Gaillard, J.-F.; Stair, P. C. *J. Am. Chem. Soc.* **2003**, *125*, 14284.
(8) Burns, R. G.; Burns, V. M. Mineralogy. In *Marine Manganese Deposits*; Elsevier Oceanography Series 15; Glasby, G. P., Ed.; Elsevier: Amsterdam, 1977; p 185.
(9) Manceau, A.; Gorshkov, A. I.; Drits, V. A. *Am. Mineral.* **1992**, *77*, 1144.
(10) Manceau, A.; Combes, J. M. *Phys. Chem. Miner.* **1988**, *15*, 283.
(11) Bargar, J. R.; Tebo, B. M.; Villinski, J. E. *Geochim. Cosmochim. Acta* **2000**, *64*, 2775.
(12) More than 98% of the manganese in deep ocean nodules was reported [Piper, D. Z.; Basler, J. R.; Bischoff, J. L. *Geochim. Cosmochim. Acta* **1984**, *48*, 2347] to be present as Mn(IV).
(13) O'Day, P. A. *Rev. Geophys.* **1999**, *37*, 249.
(14) De Mishima, B. A. L.; Ohtsuka, T.; Sato, N. *J. Electroanal. Chem.* **1988**, *243*, 219.
(15) Bernard, M. C.; Goff, A. H. L.; Thi, B. V.; DeTorresi, S. C. *J. Electrochem. Soc.* **1993**, *140*, 3065.
(16) Ammundsen, B.; Burns, G. R.; Islam, M. S.; Kanoh, H.; Roziere, J. *J. Phys. Chem. B* **1999**, *103*, 5175.
(17) Hwang, S.-J.; Park, H.-S.; Choy, J.-H.; Campet, G.; Portier, J.; Kwon, C.-W.; Etourneau, J. *Electrochem. Solid State Lett.* **2001**, *4*, A213.
(18) Julien, C.; Massot, M. *Phys. Chem. Chem. Phys.* **2002**, *4*, 4226.
(19) Stair, P. C.; Li, C. *J. Vac. Sci. Technol., A* **1997**, *15*, 1679.
(20) Spiro, T. G.; Czernuszewicz, R. S. Resonance Raman spectroscopy. In *Physical Methods in Bioinorganic Chemistry*; Lawrence Que, J., Ed.; University Science Books: Sausalito, CA, 2000; p 59.
(21) Asher, S. A.; Ianoul, A.; Mix, G.; Boyden, M. N.; Karnoup, A.; Diem, M.; Schweitzer-Stenner, R. *J. Am. Chem. Soc.* **2001**, *123*, 11775.
(22) Luo, J.; Zhang, Q.; Huang, A.; Giraldo, O.; Suib, S. L. *Inorg. Chem.* **1999**, *38*, 6106.
(23) Potter, R. M.; Rossman, G. R. *Am. Mineral.* **1979**, *64*, 1199.
(24) Gao, Z.-X.; Kim, H.-S.; Sun, Q.; Stair, P. C.; Sachtler, W. M. H. *J. Phys. Chem. B* **2001**, *105*, 6186.
(25) Pastén, P. A. Structure and Formation Kinetics of Manganese Oxides by Leptothrix discophora SP-6. Ph.D. thesis, Northwestern University, 2002.
(26) Post, J. E.; Appleman, D. E. *Am. Mineral.* **1988**, *73*, 1401.
(27) Liu, Y.; Wang, H.; Chen, G.; Zhou, Y. D.; Gu, B. Y.; Hu, B. Q. *J. Appl. Phys.* **1988**, *64*, 4651.
(28) Wells, A. F. *Structural Inorganic Chemistry*, 5th ed.; Oxford University Press: New York, 1984.
(29) Fomichev, V. V.; Kondratov, O. I. *Spectrochim. Acta, Part A* **1994**, *50A*, 1113.
(30) Ananthanarayanan, V. *J. Chem. Phys.* **1970**, *52*, 3844.
(31) Xia, G.-G. Transformation from layered to tunnel structures: Synthesis, characterization, and applications of manganese oxide octahedral molecular sieves. Ph.D. thesis, University of Connecticut, 2001.
(32) Lanson, B.; Drits, V. A.; Feng, Q.; Manceau, A. *Am. Mineral.* **2002**, *87*, 1662.
(33) Waterland, M. R.; Stockwell, D.; Kelley, A. M. *J. Chem. Phys.* **2001**, *114*, 6249.
(34) Zangmeister, C. D.; Pemberton, J. E. *J. Phys. Chem. A* **2001**, *105*, 3788.
(35) Xia, G.-G.; Tong, W.; Tolentino, E. N.; Duan, N.-G.; Brock, S. L.; Wang, J.-Y.; Suib, S. L.; Ressler, T. *Chem. Mater.* **2001**, *13*, 1585.
(36) Nakamoto, K. *Infrared and Raman spectra of inorganic and coordination compounds, Part A: Theory and applications in inorganic chemistry*, 5th ed.; John Wiley & Sons: New York, 1997.
(37) Biellmann, C.; Gillet, P. *Eur. J. Mineral.* **1992**, *4*, 389.
(38) Langille, D. B.; O'Shea, D. C. *J. Phys. Chem. Solids* **1977**, *38*, 1161.
(39) Porto, S. P. S.; Giordmaine, J. A.; Damen, T. C. *Phys. Rev.* **1966**, *147*, 608.
(40) Burns, R. G.; Burns, V. M.; Stockman, H. W. *Am. Mineral.* **1985**, *70*, 205.

(41) Mukherjee, B. *Mineral. Magn.* **1959**, *32*, 166.
(42) Bystrom, A.; Bystrom, A. M. *Acta Crystallogr.* **1950**, *3*, 146.
(43) http://webmineral.com/.
(44) http://www.zonge.com/.
(45) Mendelsohn, R.; Monse, E. U. *J. Chem. Educ.* **1981**, *58*, 582.
(46) LeDuc, H. G.; Coleman, L. B.; Chandrashekhar, G. V. *Phys. Rev. B* **1984**, *30*, 7206.
(47) Burns, G.; Chandrashekhar, G. V.; Dacol, F. H.; Foster, L. M.; Chandrasekhar, H. R. *Phys. Rev. B* **1980**, *22*, 1073.
(48) Berney, C. V. *J. Am. Chem. Soc.* **1973**, *95*, 708.
(49) Buciuman, F.; Patcas, F.; Craciun, R.; Zahn, D. R. T. *Phys. Chem. Chem. Phys.* **1999**, *1*, 185.
(50) Bish, D. L.; Post, J. E. *Am. Mineral.* **1989**, *74*, 177.
(51) McMurdie, H. F.; Golovato, E. *J. Res. Natl. Bur. Stand.* **1948**, *41*, 589.
(52) Perram, J. W. *J. Chem. Phys.* **1968**, *49*, 4245.
(53) Tian, Z.-R.; Yin, Y.-G.; Suib, S. L.; O'Young, C. L. *Chem. Mater.* **1997**, *9*, 1126.
(54) Pessall, N.; Dunlap, A. B.; Feldman, D. W. *Corrosion (Houston)* **1977**, *33*, 130.
(55) Dean, K. J.; Wilkinson, G. R. *J. Raman Spectrosc.* **1983**, *14*, 130.
(56) Chapman, A. C.; Thrilwell, L. E. *Spectrochim. Acta* **1964**, *20*, 937.
(57) Post, J. E.; Bish, D. L. *Am. Mineral.* **1988**, *73*, 861.
(58) Shen, Y. F.; Zerger, R. P.; DeGuzman, R. N.; Suib, S. L.; McCurdy, L.; Potter, D. I.; O'Young, C. L. *Science* **1993**, *260*, 511.
(59) Horák, M.; Vítek, A. *Interpretation and Processing of Vibrational Spectra*; John Wiley & Sons, Ltd.: Chichester, New York, Brisbane, Toronto, 1978.
(60) Manceau, A.; Gorshkov, A. I.; Drits, V. A. *Am. Mineral.* **1992**, *77*, 1133.
(61) Ostwald, J. *Mineral. Magn.* **1986**, *50*, 336.
(62) Bacteria need Fe, minerals (cations), and pyruvate during their growth. The content of Fe is a limiting factor for the bacterial growth under our MSVP condition. About 1 μM of Fe is known to be needed for bacteria to grow maximally in our MSVP culture. The initial Fe concentration in the MSVP before bacteria start to grow was confirmed to be less than 0.2 μM by atomic absorption spectroscopy. Bacteria stop growing after consuming all the 0.2 μM Fe. So, more than ~80% of initial concentrations of the cations is estimated to be in the aqueous solution even after bacteria stop growing.
(63) Laberty, C.; Suib, S. L.; Navrotsky, A. *Chem. Mater.* **2000**, *12*, 1660.
(64) Post, J. E. *Proc. Natl. Acad. Sci. U.S.A.* **1999**, *96*, 3447.
(65) Takematsu, N.; Kusakabe, H.; Sato, Y.; Okabe, S. *J. Oceanogr. Soc. Jpn.* **1988**, *44*, 235.